

# A process-based model for leaf development and growth in hardneck garlic (*Allium sativum*)

Jennifer Hsiao<sup>1</sup>, Kyungdahm Yun<sup>2</sup>, Kyung Hwan Moon<sup>3</sup> and Soo-Hyung Kim<sup>2,\*</sup>

<sup>1</sup>Department of Biology, University of Washington, Seattle, WA, USA, <sup>2</sup>School of Environmental and Forest Sciences, College of the Environment, University of Washington, Seattle, WA 98195-4115, USA and <sup>3</sup>Research Institute of Climate Change and Agriculture, National Institute of Horticultural & Herbal Science, Rural Development Administration, South Korea

\*For correspondence. E-mail: soohkim@uw.edu

Received: 5 April 2018 Returned for revision: 6 June 2018 Editorial decision: 26 March 2019 Accepted: 5 April 2019  
Published electronically 23 May 2019

- **Background and aims** Phenology and morphology are two major aspects of crop growth models. A new process-based model built for hardneck garlic (*Allium sativum*) is presented, focusing on phenology and morphology processes and how they translate to whole-plant growth. The tight coupling between the two processes and their dynamic changes throughout the growing season were captured while incorporating storage effects and reproductive aspects unique to bulbous crops.
- **Methods** Non-linear temperature dependences of leaf development were integrated into the model and dynamically coupled with changes in leaf growth throughout the growing season. Bulb storage effects on leaf development and photoperiod effects on the vegetative-to-reproductive transition were also incorporated. The model was parameterized with data from a set of experiments and the literature, while its performance was tested with additional observations that had not been used for parameterization under a range of environmental conditions, management practices and cultivar choices.
- **Key Results** The model successfully captured the dynamic nature of leaf development and growth in garlic plants throughout the growing season. It simulated with reasonable accuracy the timing of leaf initiation, maturation and senescence, as well as changes in green leaf area over time. Most parameters were relatively stable across cultivars, and parameter sensitivity tests revealed the importance of bulb storage effects.
- **Conclusions** The model embodies a novel approach to capture the phenology and morphology of garlic under a range of environments, genotypes and management practices. The process-oriented nature of the model and inclusion of storage effects set the foundation for bulbous crop growth simulations, allowing the understanding and discovery of key processes that coordinate and integrate the dynamics of growth and development from organ to whole plant, with implications for crop improvement programmes while opening opportunities for modelling other bulbous crops.

**Key words:** Garlic, *Allium sativum*, crop simulation model, phenology, morphology, physiology, bulb storage.

## INTRODUCTION

Process-based simulation models are models that formally describe known or hypothetical cause–effect relationships between physiological processes and some driving factors in the environment (Chuine and Régnière, 2017). Crop models developed under such approaches serve as useful tools to understand how environment and management can influence crop growth and yield. This information can aid agricultural management decisions for improved resource use efficiency, better crop quality and higher yield. The mechanistic relationship between climate factors and crop growth described within these models also provides insights into projected changes in yield under future climate conditions, identifying the potential vulnerability within future crop production and setting the foundation for mitigation and adaptation practices.

Research groups have developed crop simulation models for various agronomic and horticultural crops, with applications ranging from regional yield predictions and water, nutrient and pest management to future crop yield and global food

security projections under a changing climate (Marcelis *et al.*, 1998; Donatelli *et al.*, 2003; Jones *et al.*, 2003; Boote *et al.*, 2013; Holzworth *et al.*, 2014, 2015). Garlic is one of the oldest cultivated crops in human agricultural history (Kamenetsky, 2007). It is produced and consumed worldwide, with a steadily increasing global production that approached 26.5 million tons by the year 2016 (Food and Agriculture Organization of the United Nations, 2016). The importance of the garlic crop in agricultural history has led to an established body of botanical and horticultural literature, with detailed information on the phenological, morphological, physiological and ecological aspects of the crop (Takagi, 1989; Kamenetsky, 2007). This rich body of literature has served as a valuable resource for several modelling attempts for garlic plants that include describing carbon gain and partitioning through empirical relations of radiation use efficiency (Rizzalli *et al.*, 2002), characterizing water requirements and water use efficiency through calculating crop evapotranspiration (Villalobos *et al.*, 2004), and capturing the ecophysiological aspects of photosynthesis and transpiration through a coupled gas-exchange modelling

approach (Kim *et al.*, 2013). Modellers have also developed whole-plant process-based simulation models for the closely related bulbous crop, onion (de Visser, 1994a, b).

While these efforts are valuable in building the basis for modelling garlic plants, little work has focused on capturing the phenological and morphological processes of the crop, two key aspects in crop modelling. Phenology sets the timing of development and transition between developmental stages while morphological development (e.g. leaf unfolding and expansion) closely follows phenology, tracking the structural changes within the modelled plant in terms of total leaf area and whole-plant architecture. These two modelling aspects determine the timing and transition between different developmental stages and the gain and loss of green leaf area available for physiological processes, as well as the changes in whole-plant structure throughout development. Both processes provide critical information in determining carbon gain and partitioning that improves final yield simulations. Phenology and morphology have been considered in models developed for other bulbous crops, such as onions (de Visser, 1994a), but while the two crops belong to the same genus, several key differences in propagation method, sensitivity to environmental cues and the timing of flowering and bulbing make them difficult to directly compare (Lopez-Bellido *et al.*, 2016).

Process-based models commonly describe phenology based on the concept of thermal time; this approach tracks heat accumulation over time through thermal units such as growing degree-days (McMaster and Wilhelm 1997). Growth and development progress by accumulating heat units, transitioning through developmental stages specific for each crop. This method captures plant growth and development in a simplistic manner, with an assumption of a linear temperature response for growth and development when these processes are often non-linear. Alternative approaches, such as a  $\beta$ -distribution model, represent the temperature responses as a non-linear relationship and have shown success in various crop simulation models, especially in capturing the negative effects of excess heat or chilling on plant development (Yin *et al.*, 1995; Kim *et al.*, 2012).

Changes in canopy architecture closely track phenological development. Total green leaf area dictates key physiological processes such as photosynthesis, carbon gain and dry mass accumulation, as well as transpiration and water relations of the whole plant. Scaling up from individual leaves to the whole plant, canopy morphology further modifies carbon and water physiology by changing the proportions of sunlit and shaded leaves inside the canopy (de Pury and Farquhar, 1997). Methods of modelling green leaf area range in complexity. Some examples include applying simple discontinuous functions or regression models in earlier model developments (Baker *et al.*, 1975; Dale *et al.*, 1980), combining the concept of specific leaf area with carbon gain and partitioning (Penning de Vries *et al.*, 1989; Marcelis *et al.*, 1998), or using functional-structural modelling methods that describe plant structure details such as the branching system, leaf angle and leaf curvature (Allen *et al.*, 2005; Godin and Sinoquet 2005; Vos *et al.*, 2010). An alternative modelling approach is to simulate green leaf area independently of carbon physiology, focusing instead on the temperature dependence and water relations of leaf expansion

(Yang *et al.*, 2009; Kim *et al.*, 2012). This approach provides flexibility in addressing the dynamic responses of leaf growth in relation to the surrounding environment. It also allows the input of morphological observations on leaf length and width distribution throughout the plant to further constrain leaf elongation and expansion.

As a bulbous crop, garlic plants have several unique phenological and morphological aspects that are not often considered in common crop models. Post-harvest, garlic cloves experience both dormancy and post-dormancy growth during the storage period prior to planting (Takagi, 1989). Post-harvest physiology not only affects plants during the storage period but also the phenological and morphological processes after planting and sprouting. Takagi (1989) showed that both temperature and duration of bulb storage affect sprouting time of garlic plants, as well as leaf appearance rate after sprouting. While storage conditions are critical for bulbous crops, models rarely link storage conditions with subsequent phenological developments. Initiation of the inflorescence (also known as the scape) is another unique process in garlic plants, indicating the transition between vegetative and reproductive stages. This transition marks the end of leaf development, and overlaps with the bulbing phase (Lopez-Bellido *et al.*, 2016), inducing competition for carbohydrates between the scape and bulb (Rosen and Tong, 2001). Capturing the time point of scape initiation is therefore critical in characterizing the transitions between phenological stages and the changes in carbon allocation patterns.

In this study, we report a new process-based crop model for hardneck garlic with an emphasis on modules simulating phenological and morphological processes. Using a flexible  $\beta$ -distribution function, the model captures the temperature response of individual leaf development. The model also accounts for bulbing phenology and floral development in conjunction with photoperiod effects throughout entire phenological stages based on the latest BBCH (Biologische Bundesanstalt, Bundessortenamt and Chemische Industrie) scale specific for the garlic plant (Lopez-Bellido *et al.*, 2016). In addition, we incorporated the effect of storage on the postharvest physiology of garlic cloves, and further effects on leaf development and growth – effects that are unique to bulbous crops. In synchrony with phenology, we dynamically tracked the temperature dependence of leaf elongation for individual leaves, the leaf length distribution of the whole plant and the allometric relationship between leaf length and leaf area to simulate changes in green and senescent leaf area throughout the crop life cycle. Finally, we parameterized the model with multi-year and multi-location field observations of leaf growth and development and validated the model with data independent of those used for parameterization. Our specific objectives were (1) to construct a new process-based model for hardneck garlic with an emphasis on phenology and morphology processes and the coupling between them; (2) to parameterize and test the model with field-based leaf phenology and morphology measurements; (3) to identify strengths and weaknesses in the current model structure for application and future improvement; and (4) to better understand key processes and traits within the development and growth of a garlic plant, and their implications for final crop yield simulations.

MATERIALS AND METHODS

Model overview

We developed a whole-plant process-based crop simulation model for hardneck garlic. The model consists of three main components: phenology, morphology and physiology (Fig. 1). Our work presented here focuses on parameterization and testing of the phenology and morphology modules. The phenology module tracks plant development throughout the growing season, starting from the storage period during the bulbous stage, then leaf development during the vegetative stages, flowering and bulbing during the reproductive stage, and finally senescence and death. In addition, we incorporated aspects of storage effects and post-harvest physiology into the phenology module to capture some of the unique

characteristics of bulbous crops that are rarely considered in other crop models. During the vegetative growth of the crop, we characterize the changes in leaf length distribution throughout the whole plant in synchrony with phenology and track how individual leaves elongate and expand to mature throughout development. The synchronized interaction between the phenology and morphology modules allowed us to capture the leaf growth dynamics of a whole plant in a flexible manner, setting the foundation for simulations of photosynthesis and carbon gain in the physiology module. The model is written in the computer language C++ and is executable in the Windows or Mac OS environment. The source code and other files associated with the simulations and figures within this manuscript are available via an open-access repository: Zenodo (<https://doi.org/10.5281/zenodo.2598781>) as release version 0.1.10. Model simulations require a weather file that includes hourly input of

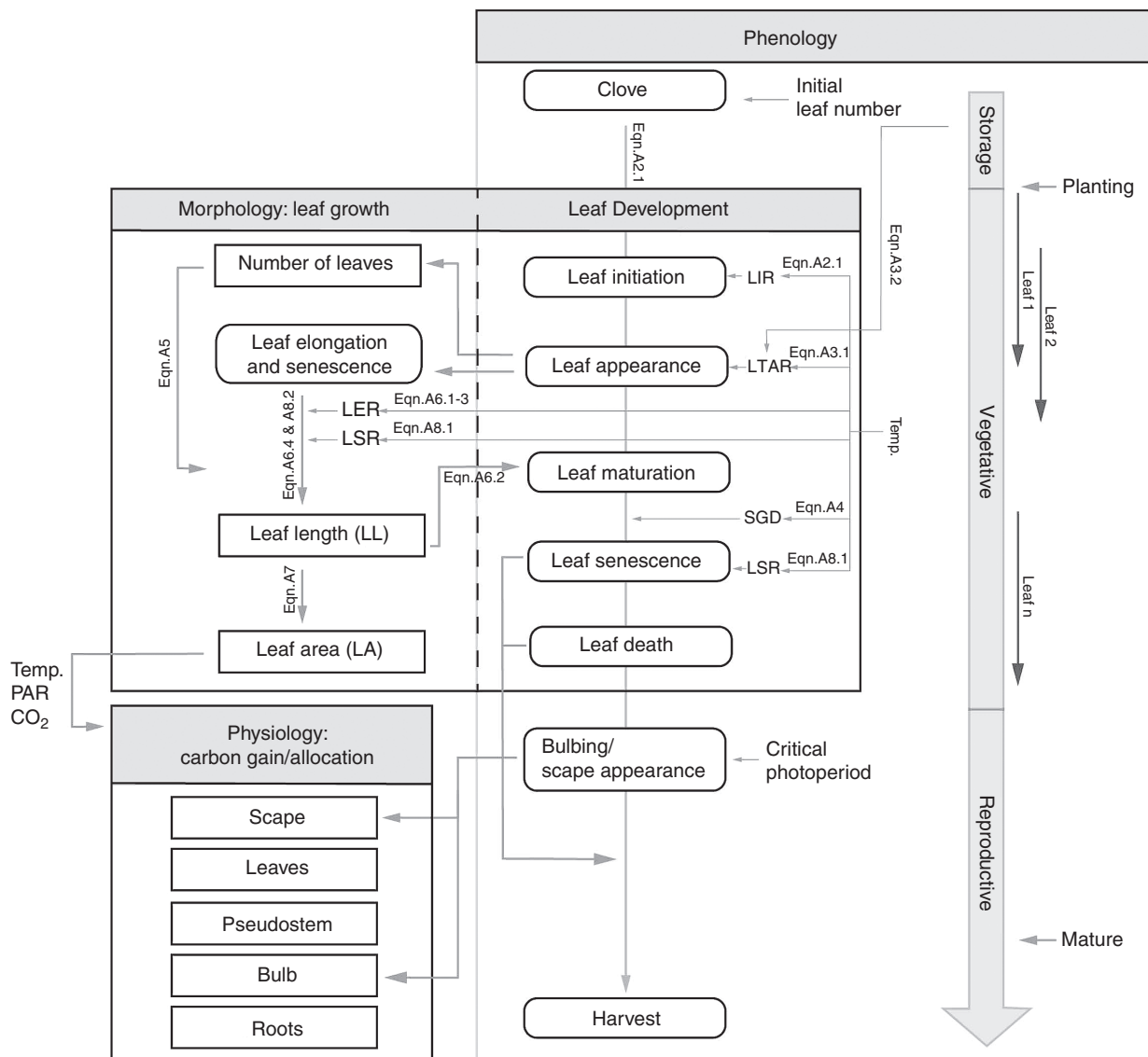


FIG. 1. Relational diagram of model structure and information flow. We focused on describing leaf development (phenology) and leaf growth (morphology) within our study. Other components include an overall phenological timeline throughout the life cycle of the plant, and a carbon gain and partitioning module that calculates gas exchange and carbon gain and allocates it to individual plant parts in synchrony with the phenological stage. Detailed descriptions of equations, parameters and parameter values are listed in Appendix A and summarized in Appendix B.

air temperature, relative humidity, wind speed and solar radiation. Users can also provide additional details of management practices and cultivar information to customize the initial state of the simulation. A more detailed description of the model can be found in [Appendix A](#).

#### Model parameterization

We used data from the literature and field-plot experiments on detailed leaf development phenology and morphological characteristics of individual leaves throughout the growing season to parameterize the model.

**Plant materials and experimental setup.** In the year 2014 we purchased 90 seed cloves of two Asiatic garlic seed clove cultivars, *Allium sativum* ‘Shantung Purple’ (SP) and ‘Korean Mountain’ (KM), from Hood River Garlic (Hood River, OR, USA). We kept the seed cloves under a 5 °C cold storage condition after they arrived in early September prior to an early (1 October 2014) and late (20 November 2014) planting in the field. The cloves were planted with a density of 55 plants m<sup>-2</sup> in three raised beds at the Center for Urban Horticulture, University of Washington in Seattle, WA, USA. We used commercially available topsoil (three-way soil mix composed of sandy soil, composted sawdust and manure) to fill the beds, fertilized the plots prior to planting with a commercial controlled-release fertilizer (14N-14P-14K) and top-dressed the soil in early February and mid-March (17N-3P-6K). We supplied a total of 240 kg ha<sup>-1</sup> N throughout the experiment, with 60 % supplied as base fertilizer and the rest as top-dressing. The plot was hand-weeded and well watered throughout the growing season. We obtained hourly weather data (air temperature, relative humidity, wind speed and solar radiation) for the growing season, required for model simulation, from an on-site weather station that is part of the Washington State University AgWeatherNet (<https://weather.wsu.edu>).

**Phenology and morphology data collection.** We recorded weekly leaf development for each cultivar and planting date combination for each individual plant and leaf, which included the timing of leaf emergence, maturation and senescence. We defined leaf emergence as the time when the leaf tip becomes visible, leaf maturation as when the leaf reaches maximal length, and leaf senescence as when >50 % of the leaf has withered and yellowed. We also tracked the date of scape appearance, which is defined as the time point when the tip of the scape becomes visible after the emergence of the last leaf. Depending on the planting date and growing season length, we conducted three to five destructive harvests throughout the growth period. We selected harvest dates that spanned different stages within the plant life cycle, but the actual dates differed between groups due to timing differences in phenological development. During each harvest, we randomly selected 15 plants from each cultivar–planting date combination and recorded leaf length, width and area for each individual leaf. We recorded whether individual leaves had reached maturity to determine whether the recorded leaf was still in the process of elongation or had reached its maximal length.

**Parameterization process.** We used the simplified  $\beta$ -distribution model (Yan and Hunt, 1999) shown in [Appendix A](#) [eqn (A1)] to describe the temperature dependence of leaf initiation, appearance and elongation. This smooth and non-linear characteristic of the  $\beta$ -function generates a bell-shaped temperature response;

the rate of these processes accelerates with temperature before reaching a plateau at an optimal temperature ( $T_{opt}$ ), at which the maximal rate is reached. Once temperature surpasses the optimum, the rate starts to decline and eventually ceases when a ceiling temperature ( $T_{ceil}$ ) is reached. We used published data on the temperature response of biomass accumulation in garlic plants from [Oh et al. \(2015\)](#) to parameterize  $T_{opt}$  and  $T_{ceil}$  in the  $\beta$ -distribution model for these processes through the non-linear least-squares approach ([Fig. 2A](#)).

Next, we used the phenology and morphology data collected in Seattle in year 2014 for cultivars SP and KM to parameterize four key parameters: maximal leaf initiation rate ( $LIR_{max}$ ), maximal leaf tip appearance rate ( $LTAR_{max}$ ), leaf elongation rate ( $LER_{max}$ ) and the stay-green duration (SG). Detailed descriptions of the model equations and associated parameters can be found in [Appendixes A and B](#). We carried out the parameterization process in consecutive steps, targeting one specific parameter during each step and minimizing the associated error calculated through root mean square errors (RMSE) and model efficiency (EF): (1) we first used the final leaf counts from all cultivar–planting date combinations to parameterize a single  $LIR_{max}$  [[Appendix B](#), eqn (A2.1)] value for all cultivars; (2) we then used the number of leaves that appeared throughout development from all cultivar–planting date combinations to generate multiple values of maximal leaf tip appearance rate influenced by storage duration (SD) ( $LTAR_{max,SD}$ ), and used a linear regression to fit a single  $LTAR_{max}$  [[Appendix B](#), eqn (A3.2)] value; (3) next, we used mature leaf counts throughout development from both cultivars to parameterize a single  $LER_{max}$  value [[Appendix B](#), eqn (A6.3)]; (4) finally, we used the number of senescent leaves throughout the growing season to parameterize cultivar-specific SG values ([Appendix B](#), eqn A4). This parameterization process is also summarized in [Table 1](#) and the associated errors and figures are given in [Table 2](#).

The parameters were held constant across cultivars with an exception for the parameter SG. Since we only had detailed phenology tracking observations for cultivars SP and KM, we pooled the dataset of these two cultivars for other cultivars (i.e. ‘Japanese Mountain’ and ‘Namdo’; see below for details) used in model testing. Also note that we used data points digitized from [Fig. 16 in Takagi \(1989\)](#) to provide samples for shorter storage durations needed for parameterizing  $LTAR_{max,SD}$  ([Fig. 2B](#)) with an assumed storage temperature of 5 °C. In addition to the linear regression used to parameterize  $LTAR_{max}$ , we used a differential evolution algorithm (Storn and Price, 1997) implemented in the SciPy package (Jones et al., 2001) to obtain a set of parameters optimized for our phenology dataset.

#### Model performance testing

We used datasets independent from those used in the parameterization process to test the model performance for different cultivars, management practices and environmental conditions. Specifically, we tested the model’s ability to simulate leaf initiation during storage as well as leaf appearance, leaf area accumulation and changes in leaf length distribution throughout the growing season. [Table 3](#) summarizes the datasets used for these various validations and the figures associated with them.

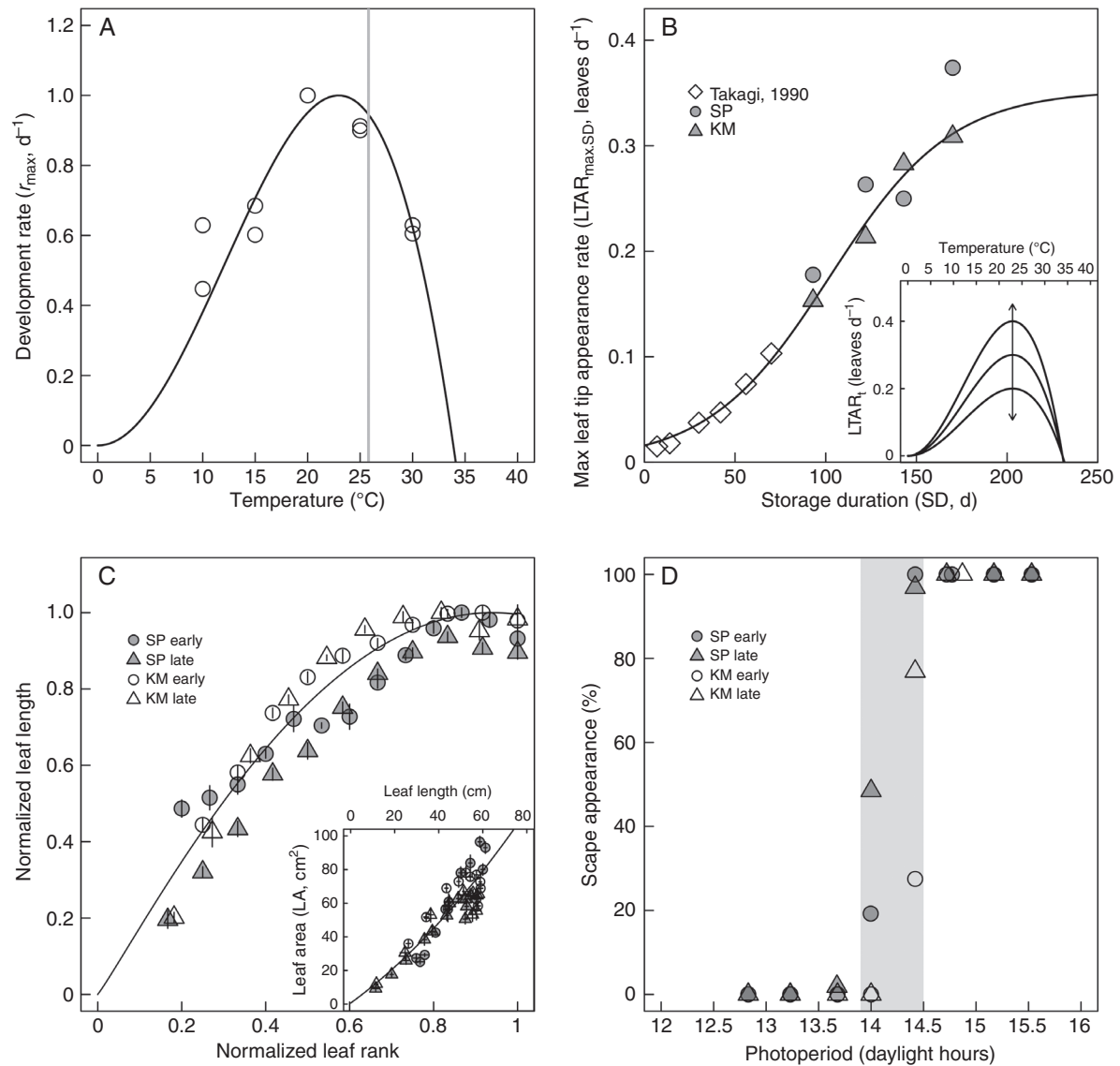


FIG. 2. Observation-derived empirical relationships within the model. (A) A  $\beta$ -distribution function used to describe the temperature response of development rate ( $1/\text{d}$ ) within our model. Circles show digitized data points from Oh *et al.* (2015) that described changes in garlic plant biomass under a range of growing temperatures. The solid grey line shows the upper limit of growth temperature within our field observations. (B) A sigmoidal function describing the relationship between storage duration and maximal leaf tip appearance rate ( $\text{LTAR}_{\max, \text{SD}}$ ); solid points show leaf tip appearance rate data collected from our study for cultivars SP and KM, and open diamonds show leaf tip appearance rate calculated from Takagi (1989). The inset shows how storage duration modifies the shape of the  $\beta$ -distribution function used to calculate  $\text{LTAR}_t$ . (C) Allometric relationship between leaf length and leaf area, and the relationship between leaf rank and final leaf length normalized by total leaf number and potential leaf length (inset). (D) Scape appearance in relation to photoperiod. For plots (C) and (D), solid symbols show results for cultivar SP and open symbols for KM; circles show data from the earlier planting date, and triangles show data from the later planting date.

**Leaf initiation during storage.** In year 2017 we purchased seed cloves of SP and KM from Hood River Garlic (Hood River, OR, USA) to identify leaf initiation during the storage period. Growers harvested the seed cloves in early to mid-July and shipped them to our facility in early August. Once they had arrived, we dissected one-third of the seed cloves through the cross-section and observed the number of leaves that had already initiated within the cloves under a dissecting microscope. We kept the remaining cloves under a  $5^{\circ}\text{C}$  cold storage condition and repeated the same procedure after 100 d of storage, and once more after 150 d of storage.

**Leaf appearance and leaf area accumulation.** We used measurements of leaf appearance and leaf area from three separate datasets to test the model's ability to capture phenological and morphological changes throughout the development of the crop. Within these datasets, we were able to robustly test the model across several cultivars and a range of planting dates, and over climate variations between growing years and locations.

We collected the first dataset for cultivars SP and KM following the same experimental setup and data collection procedure described for the parameterization dataset. The only difference in this testing dataset existed in the planting dates and year (30 October and 17 December, year 2013). We

gathered the second dataset from prior published work in our group, which included leaf development and leaf area information throughout the growing season for garlic cultivar ‘Japanese Mountain’ (JM) collected in year 2010. Detailed information on plant materials, experimental setup and data collection from this dataset are described in Kim *et al.* (2013). The Research Institute of Climate Change and Agriculture (RICCA; 33°28′ N, 126°30′ E) in Jeju Province, South Korea, provided us with the third dataset, which included phenology and morphology information of garlic cultivar ‘Namdo’ (ND) collected in the year 2010–11. Researchers from RICCA harvested the garlic bulbs in late June 2010 and stored them in shaded and ventilated conditions under room temperature in preparation for planting on 5 October 2010. They planted the seed cloves 10 cm apart with a row spacing of 18 cm in a deeply ploughed, tilled and fertilized (5.4 kg N, 5 kg P and 2.8 kg K per acre) planting bed, and covered it with a black plastic mulch-film bed prior to planting. They applied top-dress fertilization on 6 December and 30 March, which added up to a total amount of 1.2 and 0.6 kg N per acre, respectively, and followed standard agricultural practices throughout the growing season. They sampled ten plants at 14-d intervals in between 1 February 2011 and 6 June 2011. Measurements at each sampling included the fresh weight of leaves, roots, sheath and bulbs, along with the number of leaves, total leaf area, sheath and bulb diameter, clove number, length and width of the longest leaf, and scape length.

TABLE 1. Summary of the parameterization process. We parameterized maximal leaf initiation rate ( $LIR_{max}$ ), maximal rate of leaf tip appearance at optimal temperature modified by storage duration ( $LTAR_{max,SD}$ ), maximal leaf elongation rate ( $LER_{max}$ ) and the stay-green (SG) parameter in consecutive steps with different target variables, pooling and optimization methods. We collected the parameterization dataset from Seattle, USA, where we planted two garlic cultivars, ‘Shantang Purple’ (SP) and ‘Korean Mountain’ (KM) early or late in the year 2014 (see Table 3). The parameterization process was either cultivar-independent (CI) or cultivar-specific (CS), and was carried out through differential evolution (DE) or linear regression (LR)

| Parameter       | Variable                | Pooling | Method | Equation |
|-----------------|-------------------------|---------|--------|----------|
| $LIR_{max}$     | No. of final leaves     | CI      | DE     | A2.1     |
| $LTAR_{max,SD}$ | No. of leaves appeared  | CI      | DE, LR | A3.2     |
| $LER_{max}$     | No. of mature leaves    | CI      | DE     | A6.3     |
| SG              | No. of senescent leaves | CS      | DE     | A4       |

TABLE 2. Calculated RMSE and EF for model phenology and morphology outputs after parameterization and for model testing, along with their associated figures. We used filed observation data collected in two consecutive years from cultivars SP and KM for model parameterization (year 2014) and testing (year 2013)

|                                   | Parameterization (2014) |      |        | Testing (2013) |      |         |
|-----------------------------------|-------------------------|------|--------|----------------|------|---------|
|                                   | RMSE                    | EF   | Figure | RMSE           | EF   | Figure  |
| Final leaf count                  | 0.53                    | 0.89 | 3      | 0.73           | 0.43 | 5 inset |
| Leaf count throughout development | 0.81                    | 0.96 | 3      | 0.64           | 0.96 | 5 inset |
| Mature leaf count                 | 0.91                    | 0.95 | 3      | N/A            | N/A  | N/A     |
| Senescent leaf count              | 0.82                    | 0.91 | 3      | N/A            | N/A  | N/A     |
| Leaf area (cm <sup>2</sup> )      | 99.97                   | 0.46 | 4      | 87.40          | 0.63 | 5       |

Leaf length distribution throughout development. We used detailed leaf morphology data collected in the year 2010–11 at RICCA for ND to test how the model captured changes in leaf length distribution throughout development. The planting procedures for this dataset followed the ND dataset described earlier, but with greater focus on leaf length measurements, in which researchers collected weekly measurements of individual lengths of five to seven leaves starting from the top of the plant.

Model performance testing. We tested the model’s performance for (1) leaf initiation during storage, (2) leaf appearance and leaf area accumulation throughout development, and (3) changes in leaf length distribution throughout development with a range of datasets collected from different cultivars grown at other locations. We used root mean square error (RMSE) and model efficiency (EF) to quantify model performance:

$$RMSE = \sqrt{\frac{\sum_1^N (y_i - Y_i)^2}{N}} \quad (1)$$

$$EF = 1 - \frac{\sum_1^N (y_i - Y_i)^2}{\sum_1^N (y_i - \bar{y})^2} \quad (2)$$

The  $i$ th model prediction  $Y_i$  corresponds to the  $i$ th observation  $y_i$  from a total record of  $N$ , and is the average of all observation records. As a part of model testing, we also used an additional dataset collected from cultivars JM and ND to test the parameter sensitivity of  $LIR_{max}$ ,  $LTAR_{max,SD}$  and  $LER_{max}$ . We applied small perturbations to each parameter value and observed their effects on phenology and morphology outputs.

## RESULTS

### Model parameterization

Phenology and morphology field observations. Field observation data showed that leaves from cultivar SP sprouted sooner than KM leaves regardless of planting time, and sprouting time differences between cultivars spanned up to more than a month for the earlier planting date (Fig. 3). Early emergence in cultivar SP allowed for a longer growing season, providing sufficient time to develop more leaves compared with cultivar KM. We also observed this pattern within cultivars, in which an earlier planting date led to earlier leaf emergence, a longer growing

season and a greater number of leaves developed when compared with a delayed planting. After sprouting, the emergence of the subsequent leaves tracked environmental temperature, showing rapid leaf emergence under warmer conditions and delayed emergence during the winter period (Fig. 3). Leaf maturation and senescence followed a similar pattern of leaf appearance throughout the season (Fig. 3).

Total leaf area per plant increased early in the growing season as individual leaves developed and elongated (Fig. 4). Leaves that emerged earlier in the growing season did not persist throughout the entire season; as these individual leaves senesced, new leaves emerged (Fig. 3). This led to a steady increase in total leaf area that peaked between late April and early May (Fig. 4), followed by an abrupt loss in total leaf area as the overall senescence

TABLE 3. List of datasets used for model parameterization and testing

| Dataset | Location                 | Cultivar | Year | Purpose   | Figures |
|---------|--------------------------|----------|------|---|---------|
| 1       | Seattle, USA             | SP, KM   | 2014 | Parameterization  | 2, 3, 4 |
| 2       | Seattle, USA             | SP, KM   | 2013 | Testing phenology and morphology output                 | 5       |
| 3       | Seattle, USA             | SP, KM   | 2017 | Testing leaf initiation during storage                  | 6A      |
| 4       | Jeju Island, South Korea | ND       | 2011 | Testing leaf length distribution throughout development | 6B      |
| 5       | Seattle, USA             | JM       | 2011 | Testing parameter sensitivity                           | 7A, B   |
| 6       | Jeju Island, South Korea | ND       | 2010 | Testing parameter sensitivity                           | 7C, D   |

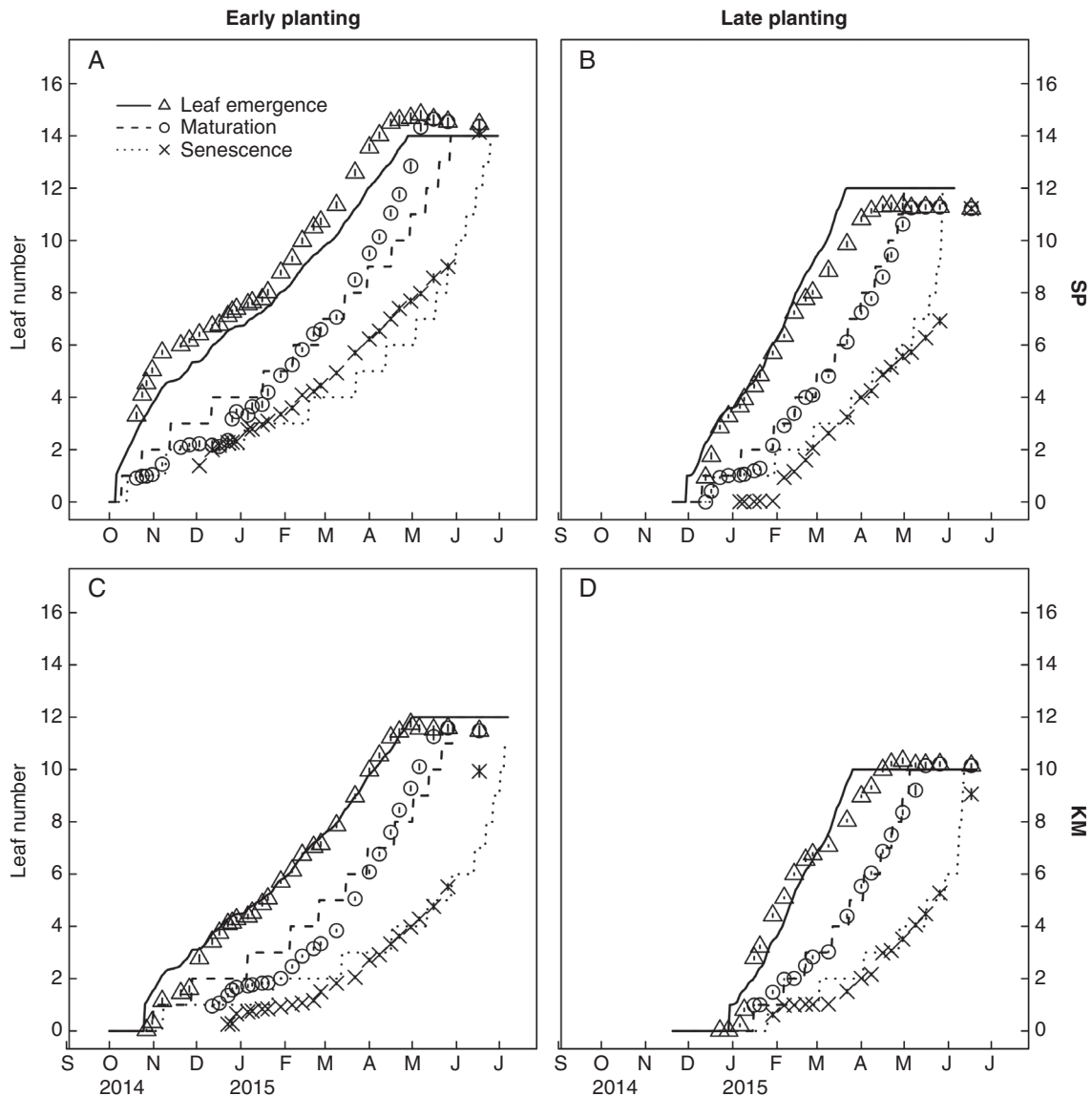


FIG. 3. Observed field data and parameterized model output of leaf development for ‘Shantang Purple’ and ‘Korean Mountain’ with an early (1 October 2014) or late (20 November 2014) planting date. Error bars represent the standard error within phenology observations ( $n = 30$ ).

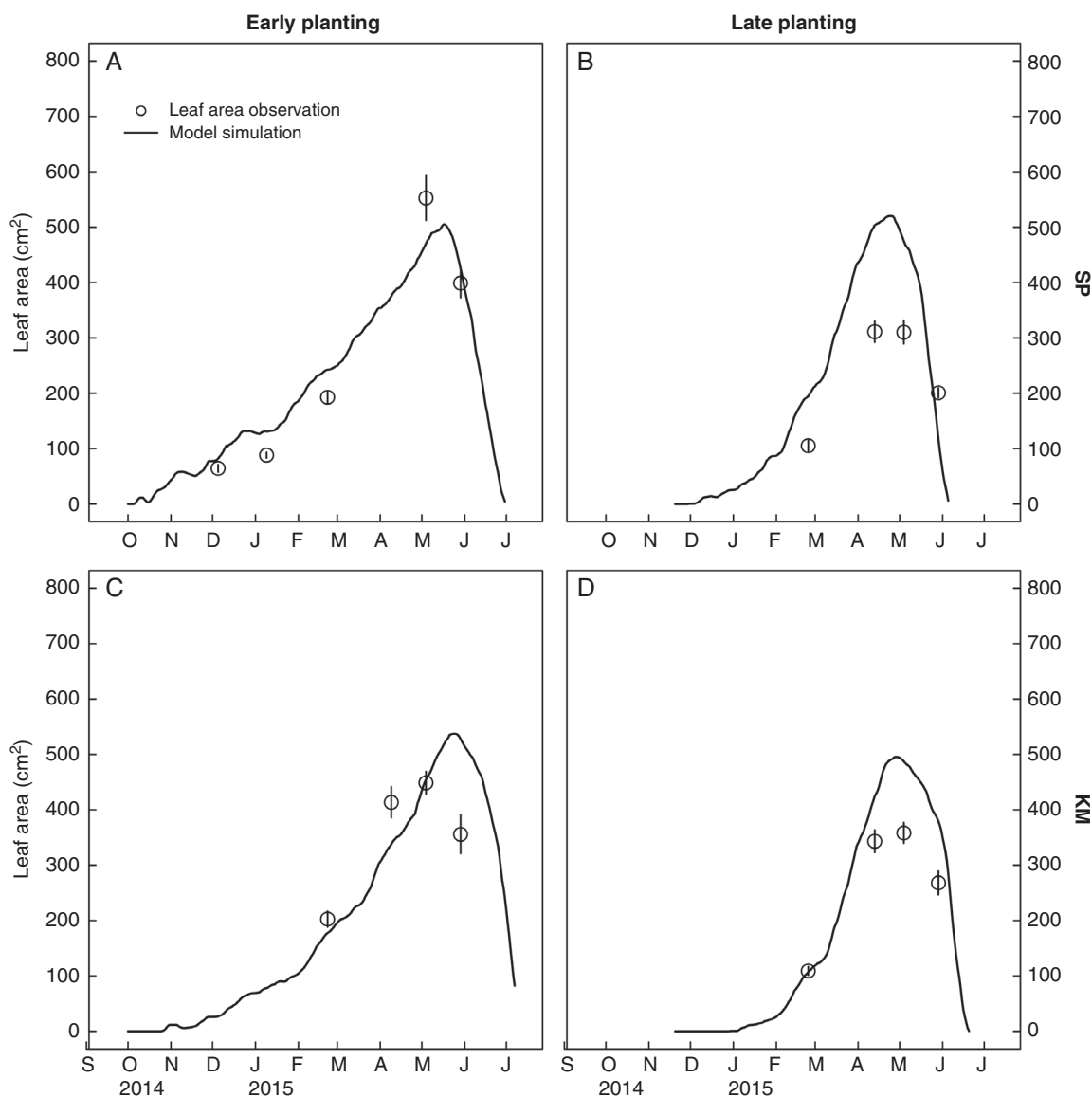


FIG. 4. Observed field data and parameterized model output of total leaf area for ‘Shantang Purple’ and ‘Korean Mountain’ with an early (1 October 2014) and late (20 November 2014) planting date. Data points represent field measurements of total leaf area at different time points throughout plant development. Error bars represent the standard error within leaf area measurements ( $n = 15$ ).

rate surpassed the emergence, elongation and expansion of new leaves (Fig. 3). Total leaf area decreased and eventually reached zero when all leaves died off towards the end of the season. Cultivar SP had greater total leaf area compared with KM (Fig. 4), which corresponded to the higher number of leaves it developed (Fig. 3). Within cultivars, an earlier planting date also led to greater total leaf area, which is likely influenced by the greater leaf number early planted crops developed (Fig. 4).

**Key parameter values and parameterization output.** We describe here the parameterization results of a few key parameters, while a full list of parameters and their values can be found in Appendix B. An optimal temperature ( $T_{opt}$ ) of 22.28 °C and a ceiling temperature of ( $T_{ceil}$ ) of 34.23 °C within the  $\beta$ -function best fitted the temperature response of biomass accumulation described in Oh et al. (2015). We adopted these values when simulating leaf initiation,

appearance, elongation and senescence (Appendix B); under  $T_{opt}$  an estimated maximum of 0.1003 and 0.4421 leaves initiated ( $LIR_{max}$ ) and appeared ( $LTAR_{max}$ ) per day, respectively, and the maximal rates of leaf elongation ( $LER_{max}$ ) and leaf senescence ( $LSR_{max}$ ) were both 4.7 cm d<sup>-1</sup> for all cultivars. The parameterization results of the empirical SG parameter were cultivar-specific, with values of 1.47 and 1.84 for leaf growth duration (LGD) for SP and KM, respectively, and a shared value of 1.50 for JM and ND, indicating differences in the relation between growth duration and SG duration between cultivars.

The parameterized model captured trends in leaf initiation, maturation and senescence throughout the growing season, tracking the differences between cultivars and planting dates observed within the field (Fig. 3). The RMSE values for leaf emergence were 0.45, 0.78, 0.52 and 0.15 (leaves) for early and late planting dates for cultivar SP and early and late planting dates for KM,

respectively; RMSE values for leaf maturation were 1.28, 0.53, 0.86 and 0.36, and values for leaf senescence were 0.98, 0.80, 0.82 and 0.47 (leaves). The model also simulated the overall pattern and timing of leaf area gain and loss throughout the growing season. However, other than simulations for the early planting date of SP (Fig. 4A), the model slightly overestimated the total leaf area (Fig. 4B–D). The RMSE values for total leaf area were 54.70, 140.64, 100.14 and 94.49 cm<sup>2</sup> for the early and late planting dates for SP and the early and late planting dates for KM, respectively.

*Model performance testing*

*Phenology and morphology.* After parameterizing the model, we tested model performance in simulating phenology and

morphology with an independent set of field observations collected in different years under similar planting conditions (Table 3, dataset 3). This set of field observations showed the general trends observed in the parameterization dataset (Figs 3 and 4), in which cultivar SP showed earlier phenological development compared with cultivar KM, leading to greater leaf number development and higher total leaf area (Fig. 5). Earlier planting dates within cultivars also exhibited this pattern. Model testing showed that the model captured the pattern of leaf emergence throughout the growing season as well as the final number of leaves developed under weather, storage and planting conditions different from those used for parameterization. The RMSE values were 0.63, 0.47, 0.64 and 1.05 d for the early and late planting dates of SP and the early and late planting dates of KM, respectively (Fig. 5, inset). The model also captured the

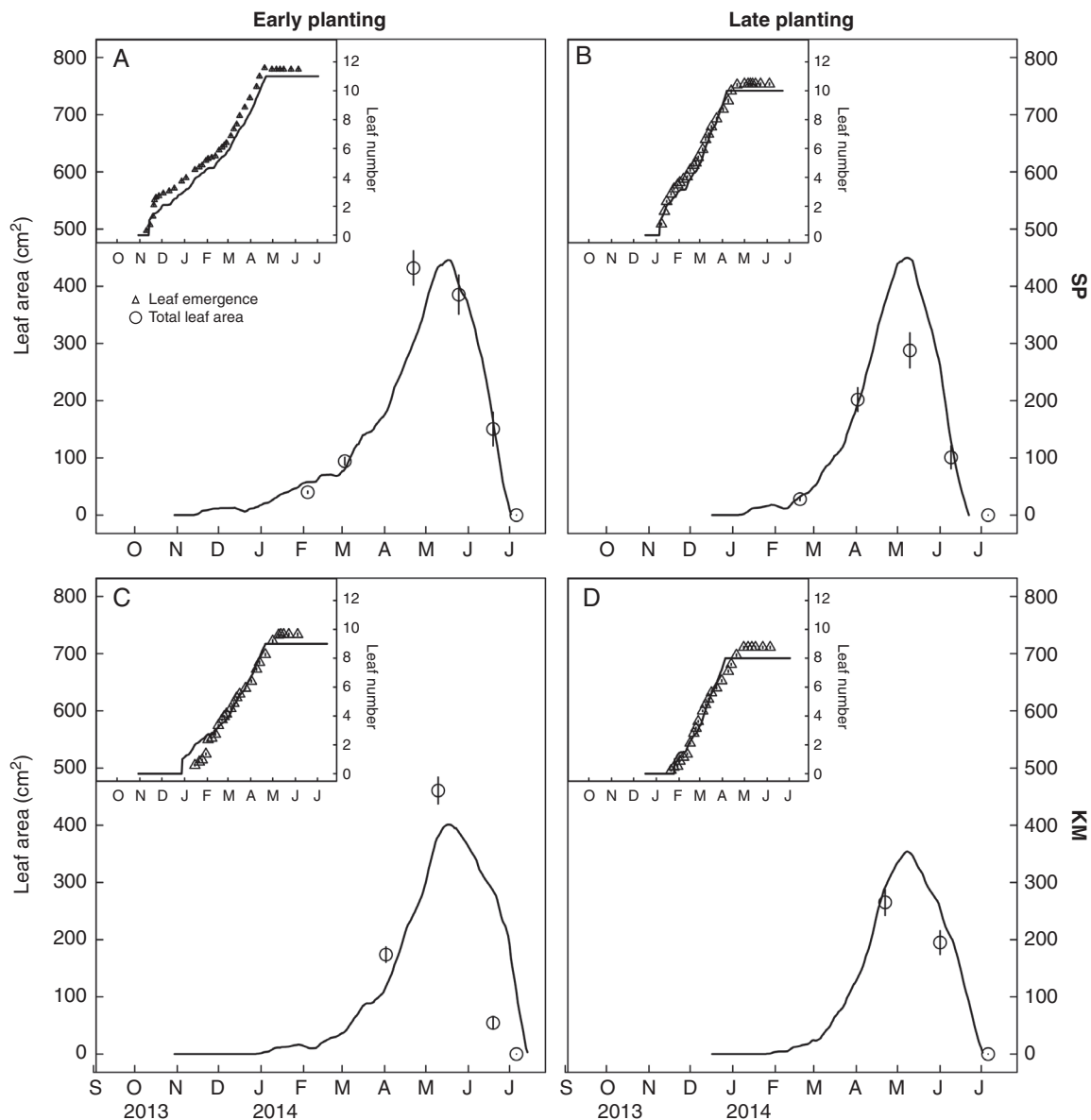


FIG. 5. Observed field data tested against model output of leaf area (main plot) and leaf emergence (inset) for ‘Shantang Purple’ and ‘Korean Mountain’ with an early (30 October 2013) and late (17 December 2013) planting date. Error bars represent the standard error within leaf emergence observations and leaf area measurements ( $n = 30$  and  $n = 15$ , respectively).

development of total leaf area throughout the growing season. The model output corresponded with field measurements in terms of timing and value of total leaf area gain, peak and loss, with RMSE values of 56.77, 81.37, 130.17 and 45.78 cm<sup>2</sup> for the early and late planting dates of SP and the early and late planting dates of KM, respectively (Fig. 5, main plots).

In addition to testing phenology (individual leaf development) and morphology (total leaf area) outputs, we also tested two processes within the model critical for phenology and morphology simulations: leaf initiation during storage [Appendix B, eqn (A2.1), Table 3 dataset 2], and the relationship between leaf rank and leaf length throughout development [Appendix B, eqn (A5), Table 3 dataset 4]. In comparison with leaf initiation observations collected for SP and KM, the model simulated the overall range of leaf initiation during the storage period for both cultivars under a 5 °C storage temperature (Fig. 6A). The model also captured the general bell-shaped pattern between leaf rank and leaf length and tracked the changes in the early and mid-developmental stages for the cultivar ND, while it tended to slightly underestimate leaf length for higher-ranked leaves later in the season (Fig. 6B).

*New cultivars, planting conditions and parameter sensitivity.* We used data independently collected from our study to test model performance under a wider range of environmental and management conditions for different cultivars, as well as to test the sensitivity of several key parameters (Table 3, datasets 5 and 6). For cultivar JM, the default model output captured the overall pattern of leaf area development (RMSE = 144.27 cm<sup>2</sup>), with a slightly delayed leaf emergence phenology, and underestimated the final number of leaves developed (Fig. 7A, B). Parameter perturbation for  $LTA_{max,SD}$ ,  $LIR_{max}$  and  $SG$  showed that  $LIR_{max}$  was the most sensitive parameter, affecting the total number of leaves simulated as well as total leaf area (Fig. 7A, B, orange dashed line). For cultivar ND, the default model output

underestimated the leaf emergence pattern (RMSE = 2.33 d) but overestimated total leaf area earlier in the season as well as towards the end (Fig. 7C, D). Among the perturbed parameters,  $SD$  had a strong influence on leaf emergence. Increasing  $SD$  from 100 to 120 d increased the number of leaves developed, which improved model performance in representing leaf emergence phenology, but led to an overestimation of total leaf area.

## DISCUSSION

Despite the global importance of garlic, there is limited modelling work focused on this crop. Grown as a biennial bulbous crop, garlic plants have unique phenology and morphology characteristics compared with many other common crops. In our modelling approach, we incorporated the latest BBCH phenological scale developed specifically for garlic (Lopez-Bellido *et al.*, 2016) and tracked leaf development and growth on a per-leaf basis. In addition, we described in our model storage effects, post-harvest physiology, environmental cues for inflorescence initiation and its concurrence with bulbing, and how these processes affected phenology and morphology. Such mechanistic modelling approaches have gained importance in the general direction of model development (Boote *et al.*, 2013), providing the flexibility to describe and adjust to growth patterns under a range of environmental and management conditions.

In our model, leaf initiation, appearance, maturation and senescence accelerate or delay in synchrony with temperature in the surrounding environment. We adopted the simplified  $\beta$ -distribution function (Yan and Hunt, 1999) to capture this non-linearity in the developmental temperature response. Using a  $\beta$ -function over commonly used thermal time approaches such as growing degree-days allows the model to capture negative effects under temperatures that exceed the optimum, and

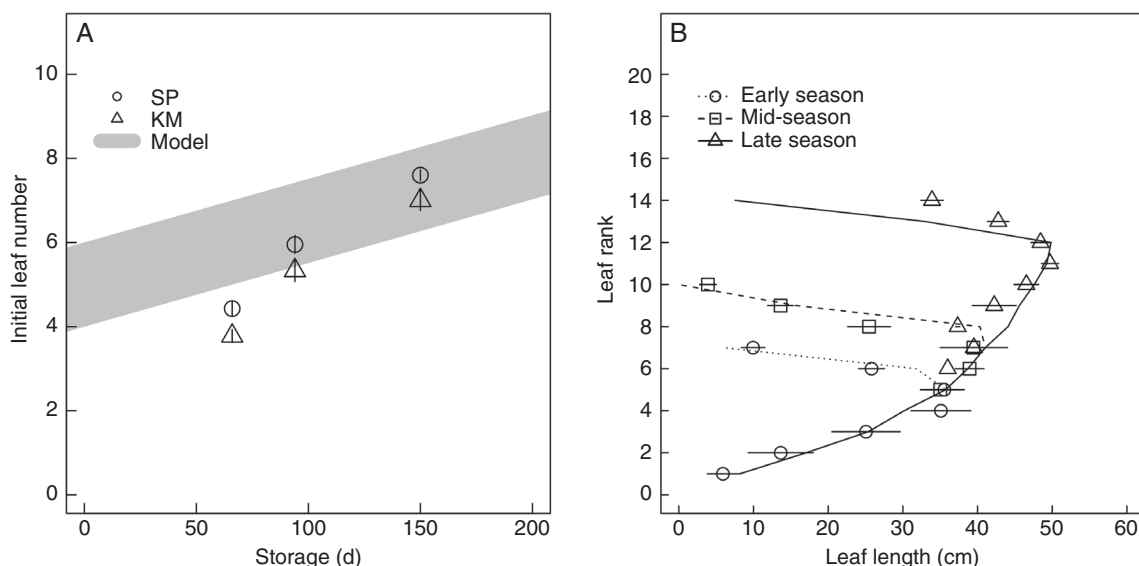


FIG. 6. Observed field data tested against model output for specific phenology and morphology measures. (A) Leaf initiation during storage for cultivars SP and KM: observed number of initiated leaves within cloves prior to planting. The shaded area shows the range of simulated initial leaf number prior to planting from the model. Error bars show the standard error within initial leaf number measurements ( $n = 5$ ). (B) Leaf length distribution throughout development: field observations of leaf length distribution within the whole plant for cultivar ND at three time points throughout the growing season: early season (7 December 2011), mid-season (7 February 2012) and late season (17 April 2012). Error bars show the standard error within leaf length measurements ( $n = 10$ ).

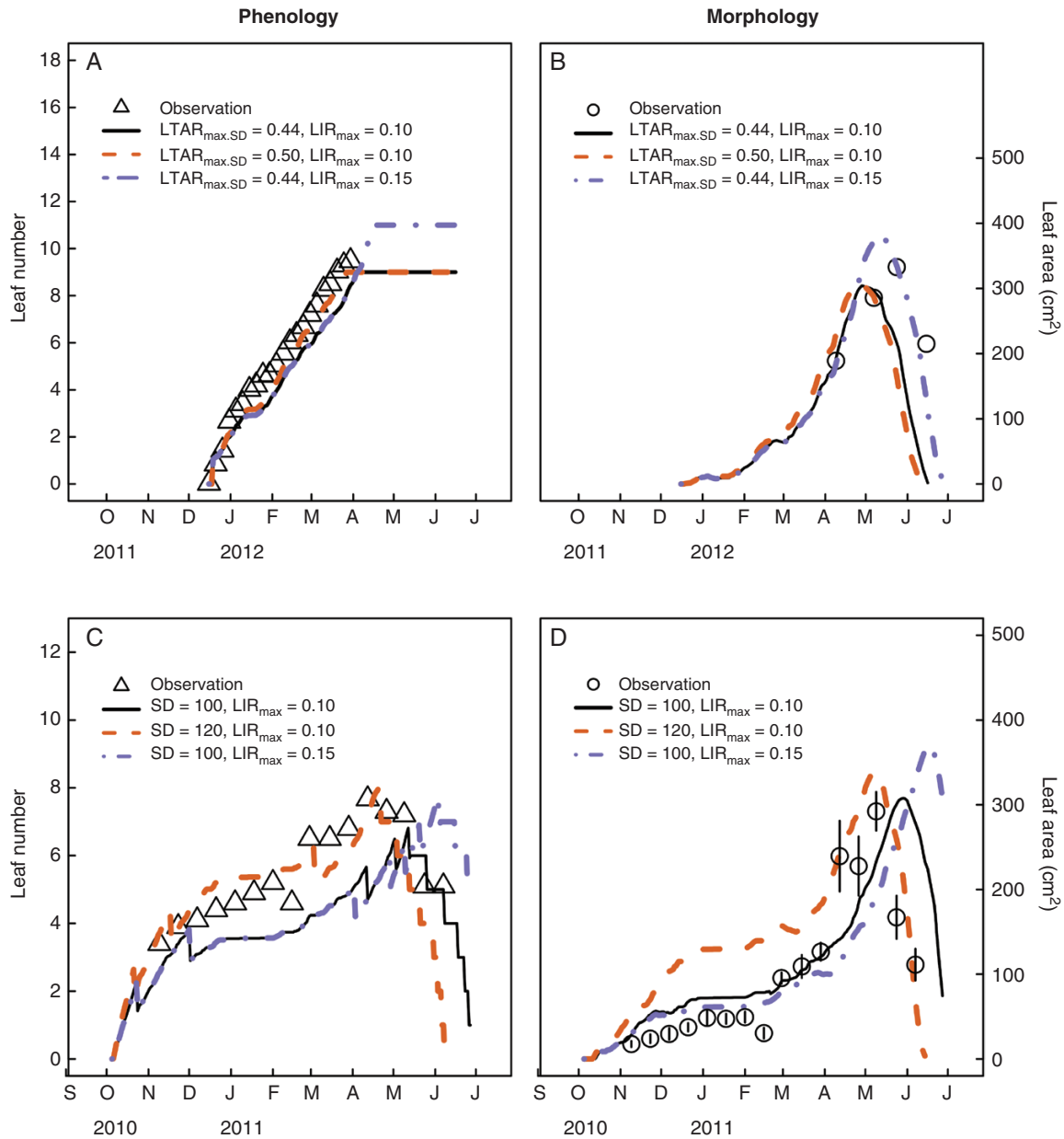


FIG. 7. Observed field data tested against model output of leaf emergence and total leaf area of cultivars JM (A, B) and ND (C, D) independently of the parameterization process. Data for ND, planted on 5 October 2010, were collected from Jeju Island, South Korea. Data for JM, planted on 11 December 2011, were collected from the same Seattle experimental site as that used in our study. Error bars for total leaf area of ND represent the standard error of leaf area observations ( $n = 16$ ). Solid lines show the default model simulation output, while dashed lines show the model outputs after perturbing parameters LTAR<sub>max,SD</sub>, SD (d) or LIR<sub>max</sub>. Descriptions of each parameter and their default values are summarized in [Appendix B](#).

provides a more realistic representation of the skewed bell-shape temperature response curve commonly observed in many biological processes with relative simplicity in terms of cardinal temperature parameters (Yin *et al.*, 1995). The  $\beta$ -function has been adopted in various process-based crop models to describe the temperature dependence of development (Kim *et al.*, 2012; Kumudini *et al.*, 2014), and captured the observations in our study well (Fig. 3 and Fig. 5 insets).

By modelling leaf development on a per-leaf basis, we dynamically tracked growth (gain in leaf length) and senescence (loss of leaf length) of individual leaves in synchrony with their

phenology, and translated this leaf length information into leaf area through an allometric relationship (Fig. 2C). Arkebauer *et al.* (1995) and Fournier and Andrieu (1998) originally proposed this general framework of modelling leaf area in which leaf expansion and senescence were driven by accumulated thermal time on a per-leaf basis; it was further adopted by several crop simulation models, such as in maize (Yang *et al.*, 2004; Kim *et al.*, 2012), sorghum (Lafarge and Tardieu, 2002), potato (Fleisher *et al.*, 2006) and sunflower (Dosio *et al.*, 2003). This leaf area simulation method differs from other common approaches, such as describing leaf area as a function of

developmental stage, deriving leaf area from carbon available and partitioned towards leaf growth together through the concept of specific leaf area, or a combination of the two (Marcelis *et al.*, 1998); it captures the dynamic temperature responses of leaf growth, and allows higher flexibility in leaf area simulations on a per-leaf basis.

The garlic plants developed a range of 10–15 total leaves within our study, with systematic differences existing between cultivar choices and planting time (Fig. 3). The maximal length of each individual leaf gradually increased with leaf rank before dropping off slightly for the last few leaves developed, resembling a skewed bell-shaped curve, which we described through a  $\beta$ -function (Fig. 2C). The flexibility within our leaf area simulation method along with the simplistic leaf arrangement within a garlic plant allowed us to incorporate this leaf length distribution information as part of the leaf area simulation. This modelling approach led to robust and dynamic leaf area simulations of individual leaves that were in tune with phenology (Fig. 6B) and tracked the gain and loss of total leaf area throughout the growing season (Fig. 4 and Fig. 5 insets).

In addition to detailed descriptions of leaf development and growth within the vegetative stage, we also focused on modelling the transition between vegetative and reproductive growth. Inflorescence formation marks the end of leaf initiation and coincides with bulbing (Lopez-Bellido *et al.*, 2016). Capturing the timing of inflorescence formation is therefore critical in determining the final number of leaves a plant will develop, as well as capturing the change in carbon allocation patterns between the vegetative and reproductive stages (Fig. 1). Temperature and photoperiod are the two main factors that influence inflorescence formation and development within garlic plants (Takagi, 1989; Kamenetsky *et al.*, 2004). In general, lower temperatures facilitate inflorescence formation, while shorter photoperiods inhibit it (Takagi, 1989). The two factors, however, show complex interactions in which the upper temperature limit for inflorescence formation increases as photoperiod decreases and vice versa (Takagi, 1989). While the use of a critical photoperiod to trigger inflorescence formation in our model simplifies the underlying physiology, photoperiod showed a clear correlation with the timing of scape appearance in our field observations. Our field observations justified this choice of a universal critical photoperiod value since all cultivar–planting date combinations showed a similar timing of scape appearance (Fig. 2D). However, whether this holds true for a wider cultivar selection would need to be tested. This modelling approach caused vegetative growth to cease at a similar time within the growing season regardless of the planting date. Earlier-planted crops therefore experienced a longer growing season that led to greater leaf development and growth, and was consistent with our field observations (Figs 3–5).

Unique to bulbous crops, a period of storage is required prior to planting. Storage duration and storage temperature are two key factors that influence the post-harvest physiology of the crop (Takagi, 1989). Storage conditions can affect dormancy and subsequent growth in substantial ways, often leading to changes in crop phenology and morphology that last well beyond the storage period. Garlic cloves are under complete dormancy only for a short period of time after harvest; once dormancy is broken, cloves regain physiological activity and can initiate leaves even when still under storage conditions (Takagi,

1989). Seed clove dissections in our experiment showed that cloves initiated more leaves prior to planting if stored longer (Fig. 6A). This phenomenon partially compensates for the shorter growing season the plant experiences if stored longer and thus planted later. Our model captures this by accounting for leaf initiation early during the storage period. This allows leaf initiation to respond to storage temperature during the storage period before switching to respond to the temperature in the growth environment after planting.

In addition, we observed that longer storage periods accelerated leaf tip appearance rate during earlier vegetative stages (Fig. 2B). This phenomenon has been described in previous literature (Takagi, 1989), and we used it together with our field observations to develop an empirical equation to show how storage duration modifies leaf tip appearance rate [Appendix B, eqn (A3.2)]. Accounting for this trait in simulating leaf tip appearance greatly improved the ability of the model to capture phenological differences in leaf appearance observed between earlier and later planting dates (Fig. 3 and Fig. 5 insets). Storage temperature is also known to affect bulb dormancy and leaf tip appearance rate; Takagi (1989) showed that lower (5–10 °C) or warmer (35–40 °C) temperatures decreased the number of days required for cloves to sprout out after planting. While we do not specifically account for storage temperature effects, flexibility in eqn (A3.2) (Appendix B) makes it possible to incorporate such capability moving forward.

With the broad set of phenology and morphology datasets used in this study, we parameterized and rigorously tested the model, spanning a range of cultivars, planting conditions and growing environments. Some datasets included more details than others; incomplete information on storage conditions, planting dates and cultivar-related parameters likely led to the discrepancy between the observations and model predictions, demonstrating the need for cultivar-specific calibration of certain parameters when applying the model to novel genotypes grown in different environmental or management conditions (Fig. 7, solid lines). Our sensitivity analysis of selected parameters identified SD as a key parameter, which affected simulations of leaf development through modifying leaf tip appearance rate (LTAR) [Appendix B, eqns (A3.1) and (A3.2), Fig. 7C] and leaf area by adjusting the timing of leaf area gain and loss (Fig. 7D). This further shows how storage conditions and post-harvest physiology can affect both crop phenology and morphology (Fig. 7D), justifying the importance of representing storage processes in crop models for bulbous crops.

Models are never perfect, but discrepancies between model simulations and observations can allude to mechanisms that are not captured within the model. It can also serve as a useful platform for hypothesis-testing of mechanisms and physiological relationships that are not yet well understood. Future model improvements would benefit from connecting the phenological, morphological and physiological components of the model to represent carbon gain and partitioning throughout development in order to simulate final yield. Expanding the model to account for below-ground root processes and responses to environmental stressors such as water and nutrient limitations is also a direction that would greatly benefit from more research. We envisage that incorporating the BBCH phenological scale for garlic will aid in communicating phenological stages between the model and observations, as well as among modellers, other scientists and growers.

## Conclusions

We developed a new process-based crop simulation model for hardneck garlic. After parameterization, the model captured the dynamics of individual leaf development and simulated green leaf area in synchrony with phenology throughout the crop life cycle for a range of cultivars, management practices and environmental conditions. Inclusion of post-harvest physiology and bulbing phenology allowed the model to account for storage and photoperiod effects unique to bulbous crops. The dynamic representation of phenology and morphology sets the foundation for modelling growth and yield in garlic plants, with the potential to be applied to other bulbous crops in the allium family and beyond. The mechanistic and integrative nature of our model assists better understanding of key processes that take part in the growth and development of garlic plants, also making it an effective platform to evaluate how these processes at the organ level are coordinated and integrated over time and space into whole-plant growth dynamics. This information is not only valuable for maximizing yield with greater efficiency under current-day production, but may also serve as an effective mitigation and adaptation tool to help identify key crop characteristics and management practices that sustain yields under stressful environmental conditions in the face of a changing climate.

## FUNDING

This work was supported in part by a Cooperative Research Program for Agricultural Science and Technology Development (PJ0127872018), Rural Development Administration, Republic of Korea.

## ACKNOWLEDGEMENTS

We thank Dr Lloyd L. Nackley and Jig Han Jeong for providing part of the data used within our analyses. We also thank Nicholas Chandler for assistance in the field and data collection. This work was supported in part by the Cooperative Research Program for Agricultural Science and Technology Development (PJ0127872018), Rural Development Administration, Republic of Korea.

## LITERATURE CITED

- Allen MT, Prusinkiewicz P, DeJong TM. 2005. Using L-systems for modeling source-sink interactions, architecture and physiology of growing trees: the L-PEACH model. *New Phytologist* **166**: 869–880.
- Arkebauer TJ, Norman JM, Sullivan CY. 1995. From cell growth to leaf growth: III. Kinetics of leaf expansion. *Agronomy Journal* **87**: 112–121.
- Baker CH, Horrocks RD, Goering CE. 1975. Use of the Gompertz function for predicting corn leaf area. *Transactions of the ASAE* **18**: 323–326, 330.
- Boote KJ, Jones JW, White JW, Asseng S, Lizaso JI. 2013. Putting mechanisms into crop production models. *Plant, Cell & Environment* **36**: 1658–1672.
- Chuine I, Régnière J. 2017. Process-based models of phenology for plants and animals. *Annual Review of Ecology, Evolution, and Systematics* **48**: 159–182.
- Dale RF, Coelho DT, Gallo KP. 1980. Prediction of daily green leaf area index for corn. *Agronomy Journal* **72**: 999–1005.
- Donatelli M, van Ittersum MK, Bindi M, Porter JR. 2003. Modelling cropping systems—highlights of the symposium and preface to the special issues. *European Journal of Agronomy* **18**: 187–197.
- Dosio GAA, Rey H, Lecoeur J, et al. 2003. A whole-plant analysis of the dynamics of expansion of individual leaves of two sunflower hybrids. *Journal of Experimental Botany* **54**: 2541–2552.
- Fleisher DH, Shillito RM, Timlin DJ, Kim S-H, Reddy VR. 2006. Approaches to modeling potato leaf appearance rate. *Agronomy Journal* **98**: 522–528.
- Food and Agriculture Organization of the United Nations. 2016. *FAOSTAT – FAO's corporate database*. <http://www.fao.org/faostat/en/#data/QC>. 26 August 2018.
- Fournier C, Andrieu B. 1998. A 3D architectural and process-based model of maize development. *Annals of Botany* **81**: 233–250.
- Godin C, Sinoquet H. 2005. Functional-structural plant modelling. *New Phytologist* **166**: 705–708.
- Holzworth DP, Huth NI, deVoil PG, et al. 2014. APSIM – evolution towards a new generation of agricultural systems simulation. *Environmental Modelling & Software* **62**: 327–350.
- Holzworth DP, Snow V, Janssen S, et al. 2015. Agricultural production systems modelling and software: current status and future prospects. *Environmental Modelling & Software* **72**: 276–286.
- Jones E, Oliphant T, Peterson P, et al. 2001. *SciPy: open source scientific tools for Python*. <http://www.scipy.org/>.
- Jones JW, Hoogenboom G, Porter CH, et al. 2003. The DSSAT cropping system model. *European Journal of Agronomy* **18**: 235–265.
- Kamenetsky R. 2007. Garlic: botany and horticulture. In: Janick J, ed. *Horticultural reviews*, Vol. 33. Wiley Online Library, 123–172.
- Kamenetsky R, Shafir IL, Zemah H, Barzilay A, Rabinowitch HD. 2004. Environmental control of garlic growth and florogenesis. *Journal of the American Society for Horticultural Science* **129**: 144–151.
- Kim S-H, Lieth JH. 2003. A coupled model of photosynthesis, stomatal conductance and transpiration for a rose leaf (*Rosa hybrida* L.). *Annals of Botany* **91**: 771–781.
- Kim S-H, Yang Y, Timlin DJ, et al. 2012. Modeling temperature responses of leaf growth, development, and biomass in maize with MAIZSIM. *Agronomy Journal* **104**: 1523–1537.
- Kim S-H, Jeong JH, Nackley LL. 2013. Photosynthetic and transpiration responses to light, CO<sub>2</sub>, temperature, and leaf senescence in garlic: analysis and modeling. *Journal of the American Society of Horticulture Science* **138**: 149–156.
- Kumudini S, Andrade FH, Boote KJ, et al. 2014. Predicting maize phenology: intercomparison of functions for developmental response to temperature. *Agronomy Journal* **106**: 2087–2097.
- Lafarge T, Tardieu F. 2002. A model co-ordinating the elongation of all leaves of a sorghum cultivar was applied to both Mediterranean and Sahelian conditions. *Journal of Experimental Botany* **53**: 715–725.
- Lizaso JI, Batchelor WD, Westgate ME. 2003. A leaf area model to simulate cultivar-specific expansion and senescence of maize leaves. *Field Crops Research* **80**: 1–17.
- Lopez-Bellido FJ, Lopez-Bellido RJ, Muñoz-Romero V, Fernandez-Garcia P, Lopez-Bellido L. 2016. New phenological growth stages of garlic (*Allium sativum*). *Annals of Applied Biology* **169**: 423–439.
- Marcelis LFM, Heuvelink E, Goudriaan J. 1998. Modelling biomass production and yield of horticultural crops: a review. *Scientia Horticulturae* **74**: 83–111.
- McMaster GS, Wilhelm WW. 1997. Growing degree-days: one equation, two interpretations. *Agricultural and Forest Meteorology* **87**: 291–300.
- Oh S, Moon KH, Koh SC. 2015. Assessment of high temperature impacts on early growth of garlic plant (*Allium sativum* L.) through monitoring of photosystem II activities. *Korean Journal of Horticultural Science and Technology* **33**: 829–838.
- Penning de Vries FWT, Jansen DM, ten Berge HFM, Bakema A. 1989. Morphological development and assimilate partitioning. In: *Simulation of ecophysiological process of growth in several annual crops*. Wageningen: Pudoc, 73–115.
- de Pury DGG, Farquhar GD. 1997. Simple scaling of photosynthesis from leaves to canopies without the errors of big-leaf models. *Plant, Cell & Environment* **20**: 537–557.
- Rizzalli RH, Villalobos FJ, Orgaz F. 2002. Radiation interception, radiation-use efficiency and dry matter partitioning in garlic (*Allium sativum* L.). *European Journal of Agronomy* **18**: 33–43.
- Rosen CJ, Tong CBS. 2001. Yield, dry matter partitioning, and storage quality of hardneck garlic as affected by soil amendments and scape removal. *HortScience* **36**: 1235–1239.
- Storn R, Price K. 1997. Differential evolution - a simple and efficient heuristic for global optimization over continuous spaces. *Journal of Global Optimization* **11**: 341–359.

- Takagi H. 1989.** Garlic *Allium sativum* L. In: Rabinowitch HD, ed. *Onions and allied crops, Vol III. Biochemistry, food science and minor crops*. Boca Raton: CRC Press, 109–157.
- Villalobos FJ, Testi L, Rizzalli R, Orgaz F. 2004.** Evapotranspiration and crop coefficients of irrigated garlic (*Allium sativum* L.) in a semi-arid climate. *Agricultural Water Management* **64**: 233–249.
- de Visser CLM. 1994a.** ALCEPAS, an onion growth model based on SUCROS87. I. Development of the model. *Journal of Horticultural Science* **69**: 501–518.
- de Visser CLM. 1994b.** ALCEPAS, an onion growth model based on SUCROS87. II. Validation of the model. *Journal of Horticultural Science* **69**: 519–525.
- Vos J, Evers JB, Buck-Sorlin GH, Andrieu B, Chelle M, de Visser PHB. 2010.** Functional-structural plant modelling: a new versatile tool in crop science. *Journal of Experimental Botany* **61**: 2101–2115.
- Yan W, Hunt LA. 1999.** An equation for modelling the temperature response of plants using only the cardinal temperatures. *Annals of Botany* **84**: 607–614.
- Yang HS, Dobermann A, Lindquist JL, Walters DT, Arkebauer TJ, Cassman KG. 2004.** Hybrid-maize – a maize simulation model that combines two crop modeling approaches. *Field Crops Research* **87**: 131–154.
- Yang Y, Kim S-H, Timlin DJ, Fleisher DH, Quebedeaux B, Reddy VR. 2009.** Simulating canopy transpiration and photosynthesis of corn plants under contrasting water regimes using a coupled model. *Transactions of the ASABE* **52**: 1011–1024.
- Yin X, Kropff MJ, McLaren G, Visperas RM. 1995.** A nonlinear model for crop development as a function of temperature. *Agricultural and Forest Meteorology* **77**: 1–16.
- Yin X, Goudriaan J, Lantinga E, Vos J, Spiertz H. 2003.** A flexible sigmoid function of determinate growth. *Annals of Botany* **91**: 361–371.

## APPENDIX A: MODEL DESCRIPTION

In our study, we developed a whole-plant process-based crop simulation model for hardneck garlic. The model consists of three main components: phenology, morphology and physiology (Fig. 1). We describe here details of each module, with a greater focus on phenology and morphology. Equations, variables, parameters, and values used within our model are summarized in Appendix B.

### Phenology

Phenology determines the timing of plant development. In our model, we describe the phenology at three different scales: the scale of a single leaf, the scale of sequential development of multiple leaves, and the scale of the overall life cycle of an individual plant (Fig. 1). Various plant properties, such as leaf area accumulation and carbon partitioning, change throughout a plant's life cycle in synchrony with phenology (Fig. 1). The phenology module therefore serves as a backbone structure within a crop model for other modules to build upon or refer to.

*Life cycle of a garlic plant.* We adopted the latest BBCH phenology scale developed specifically for garlic plants (Lopez-Bellido et al., 2016) to describe key phenological stages in the life cycle of the crop (Fig. 1). This phenology scale differs from the BBCH scale for onion and other *Allium* spp., and describes specific aspects of propagation, flowering and bulbing unique to garlic plants. In temperate regions, garlic plants are commonly planted as seed cloves in mid- to late autumn, but planting can be delayed until spring in regions with severe winters (Kamenetsky, 2007). The plants remain in a vegetative stage throughout the cool winter and early spring periods, continuously sprouting leaves before vernalization,

and photoperiod requirements are satisfied for a transition into the reproductive stage (Kamenetsky, 2007). Bulbing and scaping are two distinct phenological events that mark this transition (Fig. 1). Once environmental conditions shift to warm and dry, above-ground plant parts begin to senesce and eventually die off while bulbs below ground continue to accumulate biomass. Garlic cloves are commonly harvested when most of the leaves have senesced, and are then kept under storage conditions in preparation for the upcoming autumn planting (Kamenetsky, 2007).

Our phenology module largely focuses on the development and growth of individual leaves within the vegetative stage, which we describe through five consecutive processes: leaf initiation, appearance, maturation, senescence and finally death (Fig. 1). Accurately capturing these processes for each individual leaf sets the foundation for simulating whole-plant leaf development throughout a plant's life cycle.

*Leaf initiation and appearance.* We define leaf initiation in the model as the time point of leaf primordium formation. This process can begin as early as when the seed cloves are still in storage and the process can continue throughout the growing season. We used a generic form of a simplified  $\beta$ -distribution model (Yan and Hunt, 1999), shown in eqn (1), to describe the temperature dependence of leaf initiation and appearance:

$$\beta(x, r_{\max}, x_{\text{ceil}}, x_{\text{opt}}) = r_{\max} \left( \frac{x_{\text{ceil}} - x}{x_{\text{ceil}} - x_{\text{opt}}} \right) \left( \frac{x}{x_{\text{opt}}} \right)^{\frac{x_{\text{opt}}}{x_{\text{ceil}} - x_{\text{opt}}}} \quad (\text{A1})$$

Following the basic structure of the  $\beta$ -distribution model [eqn (A1)], we describe leaf initiation rate at time  $t$  ( $\text{LIR}_t$ , leaves  $\text{d}^{-1}$ ) as a function of air temperature at time  $t$  ( $T_t$ , °C), maximal  $\text{LIR}$  ( $\text{LIR}_{\max}$ , leaves  $\text{d}^{-1}$ ), which is achieved under an optimal temperature ( $T_{\text{opt}}$ , °C), and maximal temperature ( $T_{\text{ceil}}$ , °C), at which leaf initiation ceases:

$$\text{LIR}_t = \beta(T_t, \text{LIR}_{\max}, T_{\text{ceil}}, T_{\text{opt}}) \quad (\text{A2.1})$$

By inputting the storage temperature as  $T_t$ , this function also allows us to capture leaf initiation during the storage period.

Finally, we track the total number of leaves initiated by time  $t$  ( $N_t^{\text{init}}$ ) by integrating leaf initiation rate ( $\text{LIR}_t$ ) since germination ( $t^{\text{germ}}$ ):

$$N_t^{\text{init}} = \int_{t^{\text{germ}}}^t \text{LIR}_t \, dt \quad (\text{A2.2})$$

Following leaf initiation, individual leaves elongate and expand (described in the following Morphology section), allowing the leaves to extend out of the wrapped sheath and become visible for direct observation. We define this process as leaf tip appearance, and captured the rate of leaf tip appearance at time  $t$  ( $\text{LTAR}_t$ , leaves  $\text{d}^{-1}$ ) through a temperature-dependent  $\beta$ -function as well:

$$\text{LTAR}_t = \beta(T_t, \text{LTAR}_{\max, \text{SD}}, T_{\text{ceil}}, T_{\text{opt}}) \quad (\text{A3.1})$$

$\text{LTAR}_t$  tracks air temperature at time  $t$  ( $T_t$ , °C) through a  $\beta$ -function [eqn (A1)], while the maximal leaf tip appearance rate ( $\text{LTAR}_{\max, \text{SD}}$ , leaves  $\text{d}^{-1}$ ) achieved under an optimum temperature ( $T_{\text{opt}}$ , °C) is set as a function of storage duration (SD, days between harvest and planting):

$$\text{LTAR}_{\max, \text{SD}} = \text{LTAR}_{\max} / (1 + e^{-k(\text{SD} - \text{SD}_m)}) \quad (\text{A3.2})$$

$\text{SD}_m$  (d) indicates the storage day that corresponds to the inflection point within the sigmoidal function used to describe  $\text{LTAR}_{\max, \text{SD}}$ , in which the increase in  $\text{LTAR}_{\max}$  (leaves  $\text{d}^{-1}$ ) per increase in storage length is the greatest (Fig. 2B). The empirical coefficient  $k$  (unitless) determines the shape of the sigmoidal curve, and  $\text{LTAR}_{\max}$  represents the asymptote of the sigmoidal curve, creating a cap on  $\text{LTAR}_{\max, \text{SD}}$ .

Finally, we integrate leaf appearance rate ( $\text{LTAR}_i$ ) since germination ( $t^{\text{germ}}$ ) to track total number of appeared leaves by time ( $t$ ):

$$N_i^{\text{appr}} = \int_{t^{\text{germ}}}^t \text{LTAR}_i dt \quad (\text{A3.3})$$

*Leaf maturation and senescence.* Once individual leaves elongate and reach their potential length, the leaf matures and remains photosynthetically active for an extended period of time before the onset of senescence at  $t_i^{\text{sene}}$ . We describe this period as the stay-green duration ( $\text{SGD}_{i,t}$ , thermal units):

$$\text{SGD}_i = \text{SG} \cdot \text{LGD}_i \quad (\text{A4})$$

We determine  $\text{SGD}_{i,t}$  for leaf rank  $i$  at time  $t$  by multiplying a stay-green parameter (SG, unitless) with the thermal time required between leaf appearance and leaf maturation, defined as the leaf growth duration ( $\text{LGD}_{i,t}$ , thermal units). We based this equation on an assumption that smaller leaves would have shorter growth duration and therefore proportionally shorter leaf span, which is usually the case in grass crops such as maize (Fournier and Andrieu, 1998; Lizaso *et al.*, 2003). Once the thermal requirement for stay-green duration is fulfilled, leaves begin to senesce and eventually die off. We describe this process in detail in the following Morphology section.

*Photoperiod and reproduction.* Inflorescence initiation and development mark the transition from vegetative to reproductive stage within garlic plants. This is a critical time point in our model for two main reasons. First, once inflorescence initiates, it prevents additional leaf initiation and therefore sets a cap on the number of leaves a plant can develop; this is how our model determines the final leaf number. Second, flowering and bulbing occur simultaneously within garlic plants (Lopez-Bellido *et al.* 2016), and therefore mark a transition in carbon allocation within the crop as well. We chose a critical photoperiod of 12 h to mark this transition point (Takagi, 1989) to incorporate one of the main environmental cues for inflorescence initiation into our model (Kamenetsky *et al.*, 2004).

### Morphology

The morphology module is tightly linked with the phenological timeline. In our model, we focus on the distribution of final leaf length of individual leaves throughout the whole plant and the allometric relationship between leaf elongation and expansion. These aspects contribute to simulating the green leaf area present for light interception and carbon gain through photosynthesis within the plant.

*Leaf rank and final leaf length.* The first few leaves developed in a garlic plant are generally shorter. Leaf length increases for the subsequently developed leaves, reaching a maximum before decreasing again. Due to this bell-shaped pattern that we observed between leaf rank and final leaf length, we adopted a  $\beta$ -function to represent the leaf length distribution within the plant:

$$L_i = \beta(N, L_{\max}, N_{\text{ceil}}, N_{\max}) \quad (\text{A5})$$

We used a leaf ranking system to track individual leaves developed within the plant. The first leaf to sprout out is ranked as 1, and the ranking increases for the subsequent leaves.  $L_i$  (cm) describes the final length for the  $i$ th ranked leaf.  $L_{\max}$  (cm) represents the potential leaf length, which we defined as the length of the longest leaf within the whole plant, occurring under the leaf ranked  $N_{\max}$ .  $N_{\text{ceil}}$  describes the maximum leaf rank within the growth curve. We determined  $N_{\max}$  and  $N_{\text{ceil}}$  by using empirical parameters to scale it with a generic leaf number,  $N_{\text{generic}}$ . For our study, we set  $N_{\text{generic}}$  as ten leaves at the beginning of the simulation. If the model simulates more than ten leaves at some point during development,  $N_{\text{generic}}$  will simultaneously be updated to that higher total initiated leaf number,  $N_i^{\text{init}}$ . To simplify the parameter differences between cultivars and planting dates, we normalized the leaf-length and leaf-number-related parameters by the maximal leaf number and maximal leaf length. This normalization process allowed us to use a single set of parameters to capture the variation in total leaf number and maximal leaf length observed between cultivars and planting dates (Fig. 2C).

*Leaf elongation.* Phenology and morphology are tightly linked in our model structure. Once an individual leaf initiates [eqns (A2.1) and (A2.2)], it begins to elongate. Our model incorporates the concept of elongation age ( $\xi$ , thermal units) into a  $\beta$ -function to capture elongation for each individual leaf in sync with its phenology:

$$D_i = 1.5 \frac{L_i}{\text{LER}_{\max}} \quad (\text{A6.1})$$

$$\xi_{i,t} = \int_{t_i^{\text{init}}}^t \beta(T_t, 1, T_{\text{ceil}}, T_{\text{opt}}) dt \quad (\text{A6.2})$$

$$\text{LER}_{i,t} = \beta\left(\xi_{i,t}, \text{LER}_{\max}, D_i, \frac{D_i}{2}\right) \quad (\text{A6.3})$$

$$\text{LL}_{i,t} = \int_{t_i^{\text{init}}}^t \text{LER}_{i,t} dt \quad (\text{A6.4})$$

We first calculated the shortest time possible for an individual leaf of rank  $i$  to elongate and reach its final length [eqn (A6.1)]. We defined this time duration as the potential growth duration ( $D_i$ , thermal units) and calculated it through a linear relationship between  $L_i$  and the maximal elongation rate

( $LER_{\max}$ ,  $\text{cm d}^{-1}$ ) derived from Yin *et al.* (2003). Next, we determined the actual time required for elongation starting from the time of leaf initiation ( $t_i^{\text{init}}$ ), defined as elongation age for leaf rank  $i$  at time  $t$  ( $\zeta_{i,t}$ , thermal units), which we calculated based on the accumulated thermal units through a temperature-dependent  $\beta$ -function [eqn (A6.2)]. Then, we incorporated the information on potential growth duration ( $D_i$ ) and elongation age ( $\zeta_{i,t}$ ) into a  $\beta$ -function to calculate the actual rate of elongation [ $LER_{i,t}$ ,  $\text{cm d}^{-1}$ , eqn (A6.3)]. Finally, we integrated leaf elongation rate ( $LER_{i,t}$ ) from leaf initiation at  $t_i^{\text{init}}$  to calculate leaf length for leaf rank  $i$  at time  $t$  [ $LL_{i,t}$ ,  $\text{cm}$ , eqn (A6.4)].

*Leaf expansion.* As leaves elongate, they expand as well, accumulating green leaf area available for photosynthesis and carbon gain. We developed an allometric relationship between gain in leaf length and increase in leaf area through field observation data on leaves (Fig. 2C):

$$LA_{i,t} = a + b(LL_{i,t}) + c(LL_{i,t})^2 \quad (\text{A7})$$

We modelled green leaf area for leaf rank  $i$  at time  $t$  ( $LA_{i,t}$ ,  $\text{cm}^2$ ) as a function of leaf length ( $LL_{i,t}$ ,  $\text{cm}$ ), with empirical coefficients  $a$ ,  $b$  and  $c$ , which can be parameterized to capture morphological differences between cultivars.

*Leaf senescence.* Once the thermal requirement for stay-green duration is fulfilled [eqn (A4)], leaves begin to senesce and eventually die off. We describe this process through a  $Q_{10}$  function that allows leaf senescence rate at time  $t$  ( $LSR_t$ ,  $\text{cm d}^{-1}$ ) to accelerate with temperature:

$$LSR_t = LSR_{\max} \cdot Q_{10}^{\frac{(T_t - T_{\text{opt}})}{10}} \quad (\text{A8.1})$$

We calculate  $LSR_t$  by scaling the maximal senescence rate ( $LSR_{\max}$ ,  $\text{cm d}^{-1}$ ) that occurs at an optimal temperature ( $T_{\text{opt}}$ ,  $^{\circ}\text{C}$ ) with a  $Q_{10}$  factor. Then, we capture the reduction in leaf length during senescence for leaf rank  $i$  at time  $t$  ( $LL_{i,t}^{\text{sene}}$ ,  $\text{cm}$ ) by integrating  $LSR_t$ :

$$LL_{i,t}^{\text{sene}} = \int_{t_i^{\text{sene}}}^t LSR_t dt \quad (\text{A8.2})$$

We further derive the senescent leaf area of leaf rank  $i$  at time  $t$  ( $LA_{i,t}^{\text{sene}}$ ,  $\text{cm}^2$ ) by multiplying green leaf area for leaf rank  $i$  at time  $t$  with the ratio of  $LL_{i,t}^{\text{sene}}$  and  $LL_{i,t}$ :

$$LA_{i,t}^{\text{sene}} = \frac{LL_{i,t}^{\text{sene}}}{LL_{i,t}} LA_{i,t} \quad (\text{A8.3})$$

### Physiology

The physiology module builds upon the phenological and morphological information and describes gas exchange, carbon gain and carbon partitioning within the plant. To achieve the critical final step in modelling biomass and yield, we first linked the morphology and physiology module through the total simulated leaf area. Next, we used a coupled model of  $C_3$  photosynthesis, stomatal conductance and an energy balance equation to solve for the leaf-level photosynthetic rate at an hourly time step. Previous publications from our group documented details of this gas exchange module and illustrated the parameterization and validation processes specific for hardneck garlic (Kim and Lieth, 2003; Yang *et al.*, 2009). We then scaled up leaf-level photosynthesis to the whole-plant level using a sun-shade approach (de Pury and Farquhar, 1997; Kim *et al.*, 2012) and calculated total carbon gained after incorporating growth and maintenance respiration. Finally, we partitioned the carbon gained towards different plant parts including the roots, bulb, pseudostem, leaf blades and the scape (Fig. 1). We determined partitioning towards each plant part through observation-driven partitioning coefficients that change along with the phenological stage such that more carbon is partitioned towards vegetative structures during vegetative growth, and more towards the scape and bulb during reproductive growth.

APPENDIX B: Model Equations and Parameters

| Name  | Description  | Specification | Value  | Unit                   |
|---|--|---------------|--------|------------------------|
| Generic form of $\beta$ -function [eqn (A1)]  |  |               |        |                        |
| $\beta(x, r_{max}, x_{ceil}, x_{opt})$  | $= r_{max} \left( \frac{x_{ceil}-x}{x_{ceil}-x_{opt}} \right)^{\frac{y_{opt}}{x_{ceil}-x_{opt}}}$  |               |        |                        |
| This generic $\beta$ -function form is referenced from Yin et al. (2003) and is used in eqns (A2.1), (A3.1), (A5), (A6.1) and (A6.3).                     |  |               |        |                        |
| Phenology: leaf initiation [eqns (A2.1) and (A2.2)]   |  |               |        |                        |
| $LIR_t = \beta(T_t, LIR_{max}, T_{ceil}, T_{opt})$  |  |               |        |                        |
| $N_t^{init} = \int_{t^{germ}}^t LIR_t dt$   |  |               |        |                        |
| $LIR_t$   | Leaf initiation rate at time $t$   | —             | —      | leaves d <sup>-1</sup> |
| $T_t$   | Leaf initiation ceases when critical photoperiod (12 h) is reached   | —             | —      | —                      |
| $LIR_{max}$   | Mean air temperature at time $t$   | —             | —      | °C                     |
| $T_{ceil}$  | Maximal rate of leaf initiation at $T_{opt}$   | —             | 0.1003 | leaves d <sup>-1</sup> |
| $T_{opt}$   | Ceiling temperature at which leaf development ceases   | —             | 34.23  | °C                     |
| $N_t^{init}$  | Optimal temperature for development  | —             | 22.28  | °C                     |
|   | Total number of leaves initiated by time $t$ since germination at $t^{germ}$   | —             | —      | —                      |
| Phenology: leaf tip appearance and storage effects [eqns (A3.1), (A3.2) and (A3.3)]   |  |               |        |                        |
| $LTAR_t = \beta(T_t, LTAR_{max,SD}, T_{ceil}, T_{opt})$   |  |               |        |                        |
| $LTAR_{max,SD} = \frac{LTAR_{max}}{(1+e^{-t(SD-SD_m)})}$  |  |               |        |                        |
| $N_t^{appr} = \int_{t^{germ}}^t LTAR_t dt$  |  |               |        |                        |
| $LTAR_t$  | Maximal leaf tip appearance rate at time $t$   | —             | —      | leaves d <sup>-1</sup> |
| $LTAR_{max}$  | Maximal rate of leaf tip appearance at $T_{opt}$   | —             | 0.4421 | leaves d <sup>-1</sup> |
| $LTAR_{max,SD}$   | Maximal rate of leaf tip appearance at $T_{opt}$ modified by storage duration SD   | —             | —      | leaves d <sup>-1</sup> |
| $k$   | Inflection point in sigmoidal storage function   | —             | 0.0256 | —                      |
| SD  | Storage duration   | —             | 122    | d                      |
|   |  | —             | 170    |                        |
|   |  | —             | 93     |                        |
|   |  | —             | 143    |                        |
|   |  | —             | 117.75 |                        |
| $SD_m$  | Storage duration that leads to maximal leaf tip appearance rate  | —             | —      | —                      |
| $N_t^{appr}$  | Total number of leaves appeared by time $t$ since germination at $t^{germ}$ . Integration should take place only when it is less than or equal to $N_t^{init}$ | —             | —      | —                      |
| Phenology: leaf maturation [eqn (A4)]   |  |               |        |                        |
| $SGD_i = SG \cdot LGD_i$  |  |               |        |                        |
| $SGD_i$   | Stay-green duration of leaf rank $i$ , the thermal time between leaf maturation and the onset of senescence at time  | —             | —      | thermal units          |
| SG  | Stay-green parameter   | SP            | 1.47   | —                      |
|   |  | KM            | 1.84   | —                      |
|   |  | JM and ND     | 1.50   | —                      |
| $LGD_i$   | Leaf growth duration of leaf rank $i$ , growing degree days accumulated from leaf initiation until maturation  | —             | —      | thermal units          |
| Phenology: senescence   |  |               |        |                        |
| Once thermal requirement for stay-green duration is fulfilled, leaves begin to senesce. Senescence details are described in the Morphology section below. |  |               |        |                        |

## APPENDIX B: Continued

| Name  | Description  | Specification      | Value                           | Unit               |
|---|--|--------------------|---------------------------------|--------------------|
| Morphology: leaf rank and potential leaf length relationship [eqn (A5)]                                 |  |                    |                                 |                    |
| $L_i = \beta(N, L_{\max}, N_{\text{ceit}}, N_{\max})$   |  |                    |                                 |                    |
| $L_i$   | Potential leaf length for leaf rank $i$  |                    |                                 | cm                 |
| $i$   | Leaf rank, ranked from low to high following sprouting order   |                    |                                 | —                  |
| $L_{\max}$  | Length of the longest leaf, defined as potential leaf length   | SP, KM<br>JM<br>ND | 65<br>55<br>50                  | cm<br>cm<br>cm     |
| $N_{\text{generic}}$  | Generic leaf number that represents the total number of leaves within the whole plant. If the model simulates more than $N_{\text{generic}}$ leaves throughout development, it will be updated simultaneously to match |                    | 10                              | —                  |
| $N_{\text{ceit}}$   | Maximum leaf rank scaled to fit the growth curve   |                    | $1.64 \cdot N_{\text{generic}}$ | —                  |
| $N_{\max}$  | Leaf rank of the individual leaf that reaches the potential leaf length  |                    | $0.88 \cdot N_{\text{generic}}$ | —                  |
| Morphology: leaf elongation [eqns (A6.1), (A6.2), (A6.3) and (A6.4)]                                    |  |                    |                                 |                    |
| $D_i = 1.5 \frac{L_i}{\text{LER}_{\max}}$   |  |                    |                                 |                    |
| $\xi_{i,t} = \int_{t_{\text{int}}}^t \beta(T_r, 1, T_{\text{ceit}}, T_{\text{opt}}) dt$                 |  |                    |                                 |                    |
| $\text{LER}_{i,t} = \beta(\xi_{i,t}, \text{LER}_{\max}, D_i, \frac{D_i}{2})$                            |  |                    |                                 |                    |
| $\text{LL}_{i,t} = \int_{t_{\text{int}}}^t \text{LER}_{i,t} dt$   |  |                    |                                 |                    |
| $\xi_{i,t}$   | Elongation age for leaf rank $i$ at time $t$ , an integration of thermal days since leaf initiation ( $t_{\text{int}}$ ) throughout the elongation process   |                    |                                 | thermal units      |
| $D_i$   | Potential growth duration for leaf rank $i$  |                    |                                 | thermal units      |
| $L_i$   | Potential leaf length for leaf rank $i$ [eqn (A5)]   |                    |                                 | cm                 |
| $\text{LER}_{i,t}$  | Leaf elongation rate for leaf rank $i$ at time $t$   |                    |                                 | cm d <sup>-1</sup> |
| $\text{LER}_{\max}$   | Maximal elongation rate  |                    | 4.70                            | cm d <sup>-1</sup> |
| $\text{LL}_{i,t}$   | Leaf length for leaf rank $i$ at time $t$  |                    |                                 | cm                 |
| Morphology: leaf expansion allometry [eqn (A7)]   |  |                    |                                 |                    |
| $\text{LA}_{i,t} = a + b(\text{LL}_{i,t})^2$  |  |                    |                                 |                    |
| $\text{LA}_{i,t}$   | Leaf area for leaf rank $i$ at time $t$  |                    |                                 | cm <sup>2</sup>    |
| $a$   | Empirical coefficient  |                    | 0.6399                          | —                  |
| $b$   | Empirical coefficient  |                    | 0.9549                          | —                  |
| $c$   | Empirical coefficient  |                    | 0.0059                          | —                  |
| Morphology: leaf senescence [eqns (A8.1), (A8.2) and (A8.3)]  |  |                    |                                 |                    |
| $\text{LSR}_t = \text{LSR}_{\max} \cdot Q_{10}^{\frac{(t-T_{\text{opt}})}{10}}$                         |  |                    |                                 |                    |
| $\text{LL}_{i,t}^{\text{sene}} = \int_{t_{\text{opt}}}^t \text{LSR}_{i,t} dt$                           |  |                    |                                 |                    |
| $\text{LA}_{i,t}^{\text{sene}} = \frac{\text{LL}_{i,t}^{\text{sene}}}{\text{LL}_{i,t}} \text{LA}_{i,t}$ |  |                    |                                 |                    |
| $\text{LSR}_t$  | Leaf senescence rate at time $t$   |                    |                                 | cm d <sup>-1</sup> |
| $\text{LSR}_{\max}$   | Maximal rate of senescence at $T_{\text{opt}}$   |                    | 4.7                             | cm d <sup>-1</sup> |
| $Q_{10}$  | Factor   |                    | 2                               | —                  |
| $\text{LL}_{i,t}$   | Leaf length of leaf rank $i$ at time $t$   |                    |                                 | cm                 |
| $\text{LL}_{i,t}^{\text{sene}}$   | Senescent leaf length of leaf rank $i$ at time $t$   |                    |                                 | cm                 |
| $\text{LA}_{i,t}$   | Leaf area of leaf rank $i$ at time $t$   |                    |                                 | cm <sup>2</sup>    |
|   | Senescent leaf area of leaf rank $i$ at time $t$   |                    |                                 | cm <sup>2</sup>    |